COMMINUTION ENERGY EFFICIENCY – UNDERSTANDING NEXT STEPS

Lawrence K. Nordell[1, 3], Brandt Porter[2], Alexander Potapor[3]

1) *President Emeritus, Conveyor Dynamics, Inc., Nordell@conveyor-dynamics.con*
2) *Design Engineer, Conveyor Dynamics, Inc., Porter@conveyor-dynamics.com*
3) *Partner, Rocky-DEM, Inc., Potapov@Rocky-DEM.com*

ABSTRACT

Improving comminution efficiencies with better machine geometries and motions, improved nip angles, rock movement control, and voids regulation among rocks are some of the next steps to better machine performance.

Recent gains (~30%) using High Pressure Grinding Rolls (HPGR) and Vertical Roller Mills (VRM), in theory and practice, are based on Prof. Klaus Schönert's academic studies [1] (1979-1996) on rock breakage physics. More recently, University of British Columbia (UBC) Prof. Bern Klein's studies (2006-present) via D. Zorig Ph.D. thesis [2] further validates theory with practice from laboratory measurements used in this paper.

They demonstrated ideal rock compression breakage, within HPGR and VRM machines using a piston-die apparatus. Similar rock size range is used. The piston-die confine rock breakage behavior. However, these studies do not extend to larger rocks (> 75 mm), and do not demonstrate the influence of rock voids among bifurcation of rocks during comminution. Further, machines fed with larger rock sizes, such as gyratory, jaw, and cone crushers, are not designed or evaluated for geometry nip angle efficiency.

Herein we illustrate a performance gain of a new comminution machine (Conjugate Anvil-Hammer Mill - CAHM first presented at SAG 2011 [3]). The CAHM machine digests rock sizes 400% larger than HPGR, improves rock grip/nip geometry, better improves rock voids, improves surface wear life > 500%, and improves rock containment and slippage during compression. In all, the CAHM machine shows 22 potential improvements over the HPGR. Most importantly, CAHM shows a 50% kW-hr/ton improvement compared to the HPGR. Our studies use an advanced Discrete Element Method (DEM) computer program called ROCKY. ROCKY simulates moving boundaries, surface wear mechanics, and incorporates rock breakage physics based on the fundamentals of JKMRC T_{10} protocol [4] with tuned A x b breakage parameters.

We calibrate rock breakage in our DEM code to mimicking both UBC laboratory piston-die and HPGR comminution measurements. We then model CAHM with these known ore and machine properties.

Differences are illustrated using DEM techniques on each machine, including key points of when each:

a. Use geometry,
b. Initiate bifurcation breakage,
c. Provide a map of Particle Size Distribution (PSD) by location,
d. Illustrate the importance of controlling voids to minimize agglomeration after breakage,
e. Machine performance limits, and
f. kW-hr/ton benefit.

Key words: CAHM, comminution efficiency, comminution geometry, DEM, gyratory crusher, jaw crusher, HPGR, piston-die, nip angle, ROCKY, voids, vertical roller mill, University of British Columbia (UBC)

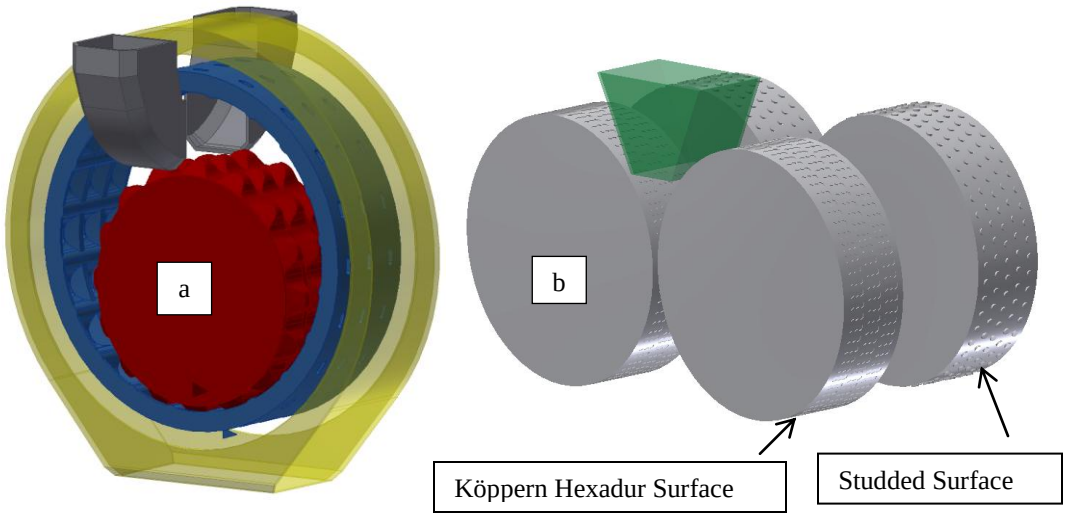

Figure 1a: CAHM – Conjugate Anvil/Hammer Mill concentric moving drums - exit-port collector hood

Figure 1b: HPGR – High Pressure Grinding Rollers – hydraulic piston maintains constant pressure at gap

INTRODUCTION

The objective of this paper is to illustrate differences between a Conjugate Anvil-Hammer Mill (Figure 1a, CAHM per Nordell [3]) and a HPGR (Figure 1b) machine, of a similar size with two surface textures, illustrated by Köppern Hexadur and Studs in their isometric views. Herein, we will demonstrate how CAHM achieves significant gain in comminution efficiency over HPGR. We used an advanced Discrete Element Method (DEM) tool trade named ROCKY [5]. ROCKY can quantify particle breakage down to 2 mm with a full Particle Size Distribution (PSD) when:

a) Comparing machine comminution efficiency in kW-hr/ton,
b) Classifying gains by particle sizes,
c) Analyzing machine power draw,
d) Predicting machine wear behavior based on shear work against comminution surfaces,
e) Measuring throughput regardless of moisture or cohesive ore properties, and
f) Quantifying rock size limit allowed.

Key features include nip angles based in surface geometries, rock compression kinematics, and ore reduction per kW, PSD, and rock voids control. We show machine validation with UBC laboratory experiments compared to DEM. We calibrate DEM breakage to piston-die and laboratory HPGR results. The HPGR uses 750 mm diameter rolls x 220 mm face width and a Hexadur surface.

Dr. Alexander Potapov developed ROCKY by rewriting CDI's older DEM 2001 code. He included a new breakage algorithm using a particle fracture model based on the noted JKMRC T_{10}, A x b comminution parameters. Here, we show many HPGR studies have validated the DEM accuracy for many comminution machines. Unlike other bond-breakage DEM models, this procedure preserves mass and volume between mother and daughter particles using Voronoi fragmentation [6]. It also keeps a history of collision energy for subsequent breakage action. We can apply further model refinements to the breakage algorithms when they are known.

Figure 2 illustrates the CAHM machine schematic, with its different comminution zones, courtesy of UBC. This illustrates the potential for direct compression without rock-liner shear slippage, except at exit port.

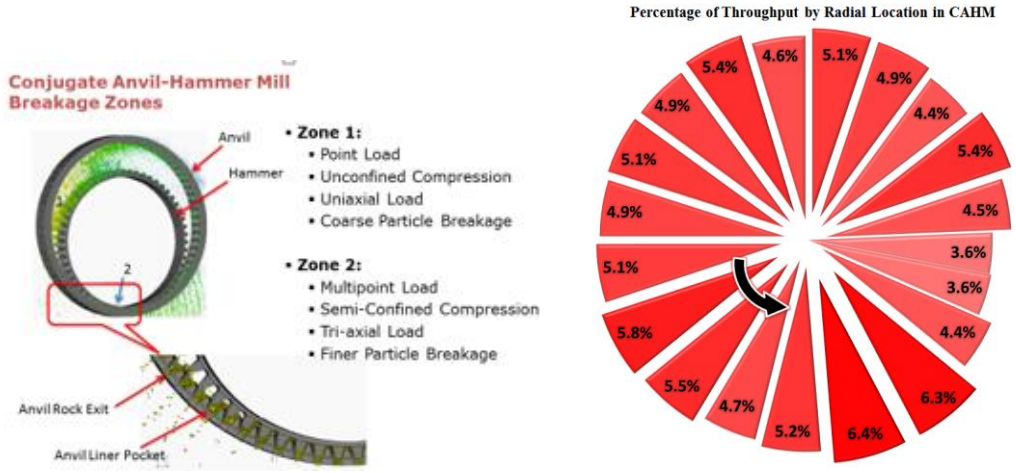

Figure 2: CAHM machine, with its piston-die action, has CCW rotation, discharge ports, and two comminution zones. Note: discharge ports set the maximum particle size to its smallest dimension. Port discharge, by location, is nearly equal throughout rotation, for one study.

The operator feeds ore at the top between Anvil and Hammer rings. The rings are rotating counter-clockwise. CAHM discharges ore at the Anvil ring port openings, before crushing noted at Zone 1, and after leaving the comminution zone. Figure 2, right image, shows the percentage of ore leaving 20 port zones around the Anvil ring showing continues discharge.

Specifically, we assert there are at least 22 areas where CAHM improves performance over HPGR including:

1. Higher throughput (1.5-2 x) for same power, PSD, and machine size – can run super critical speed
2. ~50% reduction in power at same t/h capacity
3. Larger size reduction range (20:1) is possible depending on machine and surface geometry
4. Larger rock feed size depends on machine size; for same HPGR machine (3-4x larger rock size)
5. Improved ore nip angle with many surface geometries to enhance specific PSD – min. rock slippage
6. Longer uniform rocky comminution compression range similar to Prof. Schönert's piston–die
7. Less rock particle cohesion and plastic extrusion effect = no agglomeration caking
8. Reduced ore shear work against liner wear surfaces reduces liner replacement frequency
9. Reduced ore recirculation load with much finer top size
10. PSD is improved by applying much higher roll pressure, without throughput penalty
11. Reduced particle breakage edge effect, similar to Metso HPGR flange sealing arrangement
12. Operates easily at super critical roll/ring speed and regulates production over larger speed range
13. Insensitive to moisture and cohesive product feed
14. Controls ore recycle size using extraction ports
15. Control of void spacing among particles allows for more efficient comminution
16. Improves liner durability over use of pins with larger sectional modulus of components
17. Upper limit of rock size not dependent on roller gap and limited nip angle
18. Controls lateral motion of rock under compression by using piston-die configuration
19. Improved edge sealing by Anvil ring outer flange motion moving concurrent with Hammer ring
20. Improved Anvil and Hamer ring roller stability with fixed horizontal axes
21. Can be driven with one motor
22. Faster wear replacement using liner cartridges

First, we characterize rock breakage and their parameters, by mechanical means, developed by Prof. Klaus Schönert. Next, we compare the nip angle that controls rocks at the inception of breakage (bifurcation point). Third, we compare the comminution zone of HPGR and CAHM. This demonstrates differences in pressure on working surfaces, shear work, wear, flow gradients, PSD, and surface area liberated during comminution. The CAHM machine used in our analysis is not optimized, but indicative of what is achievable.

PROF. KLAUS SCHÖNERT'S IDEAL MECHANICAL COMMINUTION MECHANISM

First, we make basic comminution comparisons disclosed by Prof. Klaus Schönert's work published in 1988 [1] where he used piston-die experiments to illustrate comminution efficiencies with packed and confined particle beds. More recently, under the guidance of UBC Prof. Bern Klein, Zorigtkhuu Davaanyam's [2] Ph.D. thesis entitled "Piston Press Test Procedure for Predicting Energy Size Reduction of High Pressure Grinding Rolls" better quantifies the laboratory method from Julius Kruttschnitt Minerals Research Center (JKMRC) T_{10} protocol per equation (eq. 1).

$T_{10} = (A)\ (1 - \exp[b])$, where $b = (-f_{mat})\ (x)\ (k)\ (E_{cs} - E_{min})$; $-f_{mat}$ is a material parameter, x is particle size, k is damage history, E_{cs} is comminution energy; E_{min} is energy to initiate crack in rock; E_{cs} & E_{min} are in kW-hr/ton (eq. 1)

JKMRC developed the well-known T_{10} and A x b parameters to predict rock PSD from these constants for most rock feed sizes, in various crushing comminution machines, down to 750 microns. The term T_{10} refers to the percent of PSD passing below 10% of screen size (mm). The term A defines the maximum degree of breakage possible and the log exponent b is the curve fit parameter of the comminution action on the PSD curve.

This rock breakage protocol is used in our ROCKY code to predict ore particle breakage based on special modified A x b parameters that include variances in rock size, shape, and history of internal rock fracture damage.

CAHM uses the piston-die configuration, in a rotating kinematic form, with the intention of minimizing confined rock pressure, and maintaining voids between rocks, while minimizing rock-to-metal slip during compression-comminution.

UBC PISTON-DIE TESTS & PSD FIT

Below we illustrate the UBC piston-die laboratory procedure that mimics Prof. Schönert's work. Later, we compare results with ROCKY. Below in Figure 3 & 4 are the UBC images of the piston-die method to size HPGR.

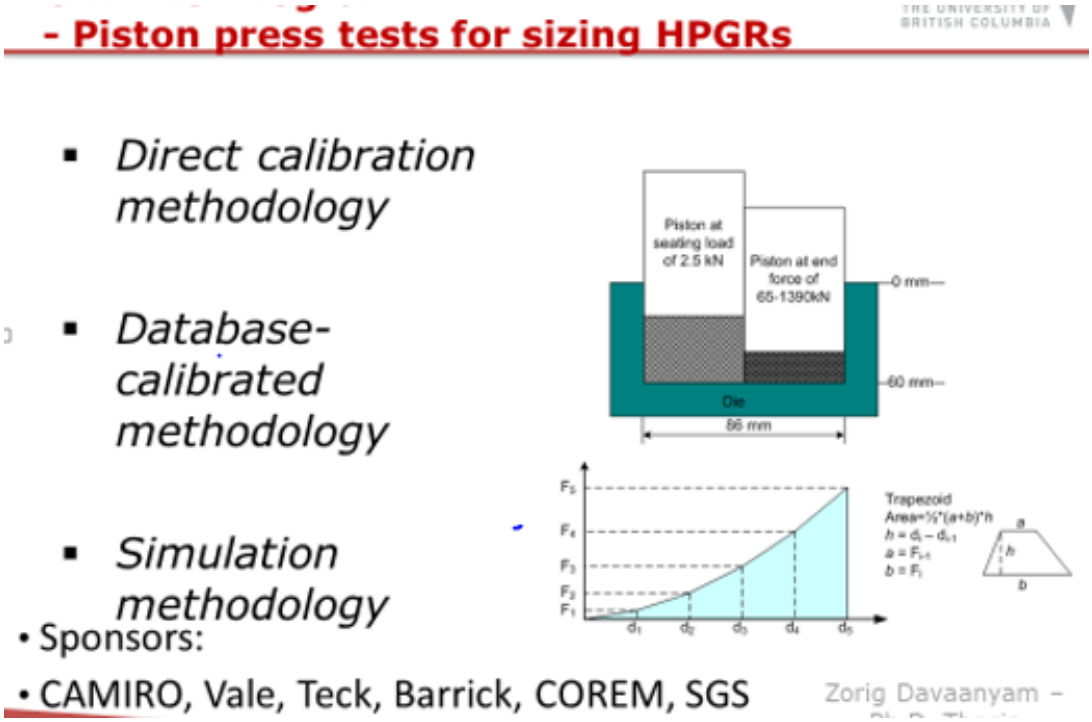

Figure 3: UBC diagrams of piston-die test protocol outline in thesis [2]

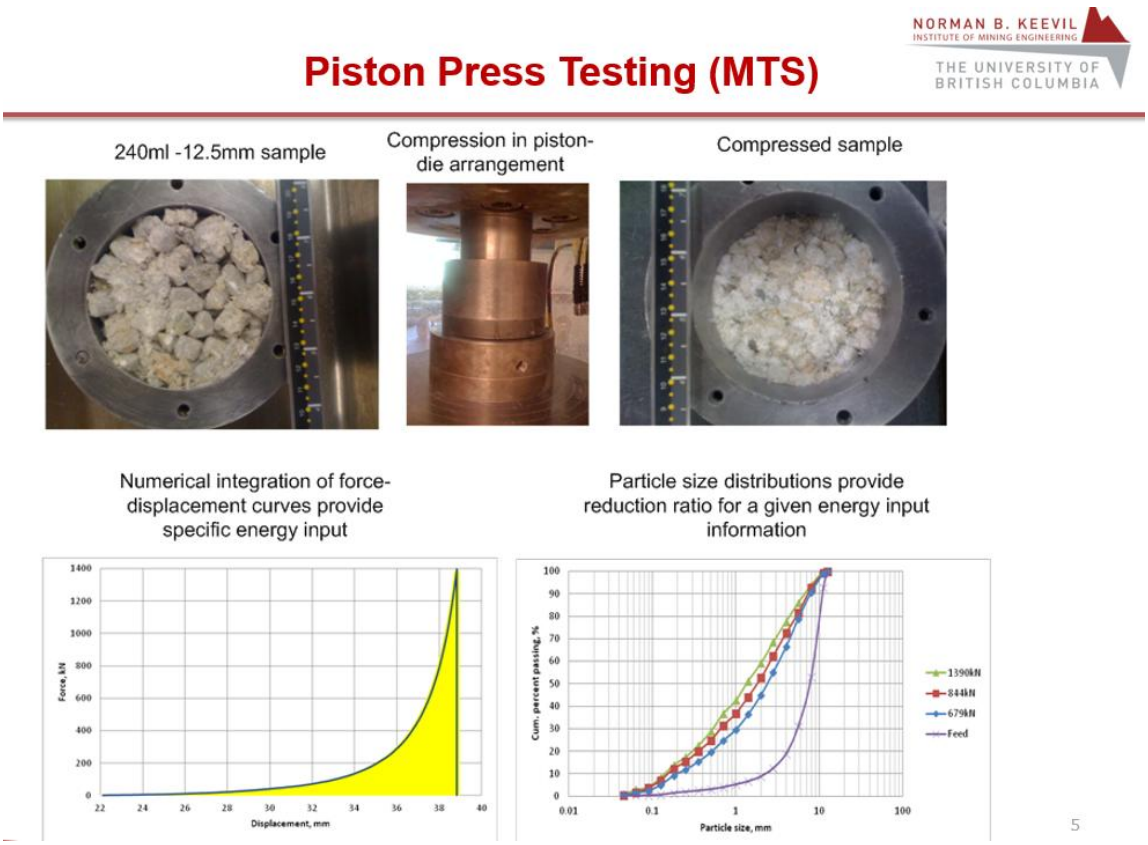

Figure 4: UBC Protocol Testing of Piston-Die Pressure vs. PSD Calibrating HPGR Throughput Performance

DEM can aid in defining A x b from the piston-die test procedure and PSD rock fragmentation for given piston stroke and pressure. The results show a direct correlation with accurate portrayal between experiment and simulation. We use the results to demonstrate, by extension, DEM can resolve performance of HPGR. Other crusher-type comminution machines, from experimental data, with greater insight than is possible by the experiments themselves.

Some key DEM observations include where comminution occurs in the piston-die apparatus, and the effects of particle wall friction with die bed depth. For the ROCKY simulations, we used a blocky-shaped rock that yields high competency. We observe comminution breaks rock from the die top down under the piston. Should this observation have any influence on HPGR behavior between the fixed and hydraulic pushing roller?

DEM may or may not accurately capture all large and small rock dynamics, but it does raise interest in yet-to-be tested theories not fully identified in the literature, such as roll shear vs. normal stress behavior in the HPGR.

JKMRC initially developed rock fracture properties using drop weight testing. JKMRC and others are making advances with continued research in larger rock size range and stress histories. This is beyond the scope of this paper. Notable researchers who are refining T_{10}, A x b include: UBC Canada [7], JKMRC Australia [4], Mintek in South Africa [8], and others [9] [10] [11] [12] [13] [14] [15]. The process is complex and offers many added avenues of research.

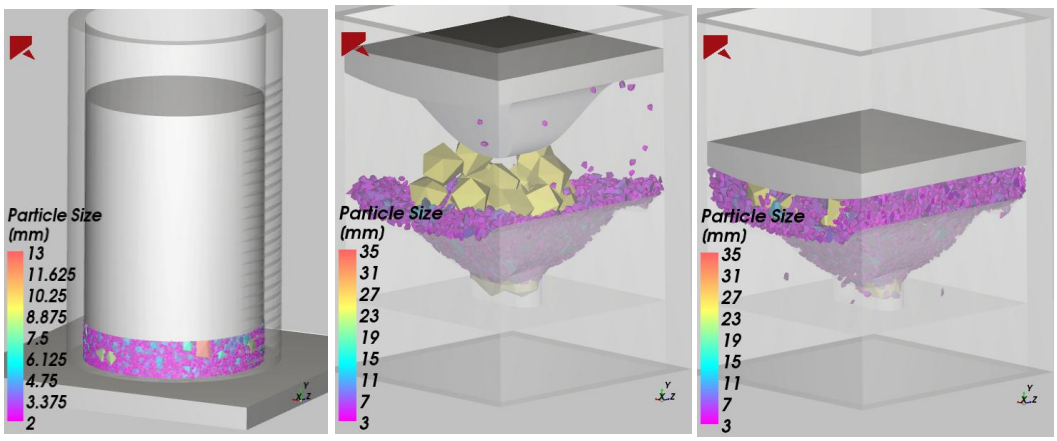

Figure 5: ROCKY Simulations for Piston-Die Analysis between UBC 86mm Diameter Die and Alternative 100 mm Square Piston with Slotted Exit Port Arrangement

In Figure 5, we examine differences between the often-used cylindrical piston-die that compresses rock to study the HPGR equivalent. Many researchers used this approach to argue that there are sufficient similarities to make the piston-die test a valuable aid in quantifying rock properties. The force vs. comminution, in this test, claims to give insight in rock fragmentation that occurs in the HPGR and other comminution devices.

Researchers should expand the piston-die test to include rock shapes and the influence of voidage between rocks by size. There is a significant drop in comminution efficiency when the voids between rocks falls below 20%. It requires a much larger force to initiate rock breakage in a packed bed.

Rock shape was recently noted for its influence in the T_{10} protocol and A x b constants in the 2015 publication indicated in the study [2]. Rock shape, with alternative 3-D aspect ratios, characterize particle size and voidage within the piston-die study for various ores.

The Figure 5 middle image illustrates both piston and die with an alternative square geometry with an exit port within the die design. Geometry selection will achieve specific rock fragmentation while maintaining a minimum voidage between rocks. The ported die will have more shear work against its working surfaces. Shear work will quantify wear action of the piston-die and exit port. We continue to study Piston-die life and rock fragmentation over the wear life cycle. This design will define the CAHM machine piston-die design from simple laboratory testing. It explains one aspect of CAHM performance gain over HPGR by maintaining rock voidage as illustrated in Figure 2.

CAHM uses a piston-die that has an exit port shown in Figure 5, right image. As rock is comminuted, fragments smaller than the exit port are released, thereby allowing the particle-to-particle voids to reach a stable percentage much lower than the standard piston-die for a given piston force, Figure 5, left side.

There are sharp difference between HPGR and CAHM. As the HPGR applies higher force, its gap closes and fragmentation increases with less and less efficiency. The gap closure is set by piston force and influences driving power.

As CAHM piston force increases, fragmentation will increase to a lesser extent, until its stroke reaches a set limit. The set limit can be controlled with a physical stop within the die. As such, the machine control is a simpler design. The piston force can be set arbitrarily high but influences neither power nor particle breakage beyond the chosen gap between surfaces. Power does not necessarily increase with piston force.

Discrete Element Method Calibration - UBC High Pressure Grinding Roll Testing

In order to match laboratory data and validate that ROCKY can accurately simulate breakage behavior of a HPGR, the various parameters were derived or extracted from the thesis paper titled "Piston Press Test Procedures for Predicting Energy-Size Reduction of High Pressure Grinding Rolls" by Zorigtkhuu Davaanyam [2]. Zorig cites many HPGR pilot scale tests and Piston-Die tests where the material information, Particle Size Distributions (PSD's) of the feed and product, energy consumption, and various other setup parameters are tracked and analyzed. For this particular case study, the material A.2 Gold (C) Ore is replicated in ROCKY. There were six tests recorded using this material: three with a pilot scale HPGR and three with a Piston-Die arrangement) at different specific pressing forces (refer to Table 1).

ROCKY supports the Gaudin-Schumann A x b and T_{10} particle breakage model. It is applied to the six test examples to define A and b using an Exponential Association Fit model. We reduce the error with least squares for the standard T_{10} exponential equation using Excel Solver per equation (eq. 1) above.

For the Gold(C) material; A = 45, b = .965, A x b = 43; where, b is derived using the assumed value for A. The A value is suspect of often being too large. It limits the exponential curvature of rock fracture behavior limited by A.

The Pilot scale HPGR used by the University of British Columbia (UBC) is a 750mm diameter x 220mm wide Köppern with Hexadur lining that enables autogenous or particle-on-particle wear to increase the life of the rolls. This study does not include liner wear, though it is worth mentioning that ROCKY can be used as a tool to determine physical wear over time. The high wear zones that occur across the face or width of the rolls, as well as through the radial breakage zone, are analyzed using surface shear work shown in detail later in this report. The rolls are modelled in 3D, using AutoCAD Inventor, with a 2.5 mm recess into the 750mm with the hex pattern starting 20mm from the edge using the dimensions shown in Figure 6. The pattern repeats 72 times and shifts by half a unit for the middle recesses. Both rolls are identical, except for recess staggering between the rolls. A 9 mm initial gap is measured from the outer most surface of the rolls.

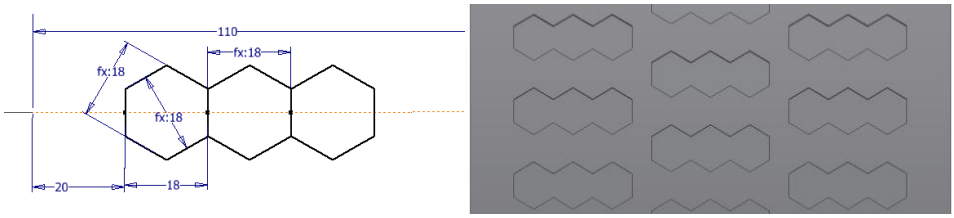

Figure 6: UBC HPGR Hexadur Surface Dimensions and Pattern Used in the Simulation

NIP ANGLE CONFIGURATIO OF FOUR COMMINUTION MACHINES

The following four itemized schematics illustrate the differences of various comminution machines and their rock nip angle relationships. According to mechanical engineering texts [14], a self-locking taper herein called the Nip Angle is about 7 degrees depending on rock surface asperities and restraining surface geometry. Note, laboratory piston-die procedure has no nip angle when compressing the rock between two platens that are confined by cylinder walls. Therefore, it does not promote understanding of machine rock-holding attributes for the four geometric concepts.

1. HPGR (dual convex roller surfaces) in Figure 7 – 24 degree included nip angle arc with Hexadur.
2. Gyratory Crusher (concave outer static surface and convex inner moving roller with smooth or serrated surfaces) Figure 8a-b – limit efficient comminution below 10-degree nip angle.
3. Vertical Roller Mill (convex roller on flat static platen) Figure 8c – moderate 14-degree nip angle
4. CAHM (concave outer moving roller surface and convex inner moving roller surface with piston-die pockets and exit ports) Figure 9 – expanded comminution zone with longest 10-degree nip angle length.

Too little study has been devoted to the influence of surface geometry vs. rock sliding control, such as Köppern Hexadur or many HPGR pin-stud dimensional placements, sizes, and patterns. Pins or studs appear to improve rock capture, by about 2-3 degrees, thereby allowing for a slightly larger rock feed size, reduces surface shear work, and improving wear.

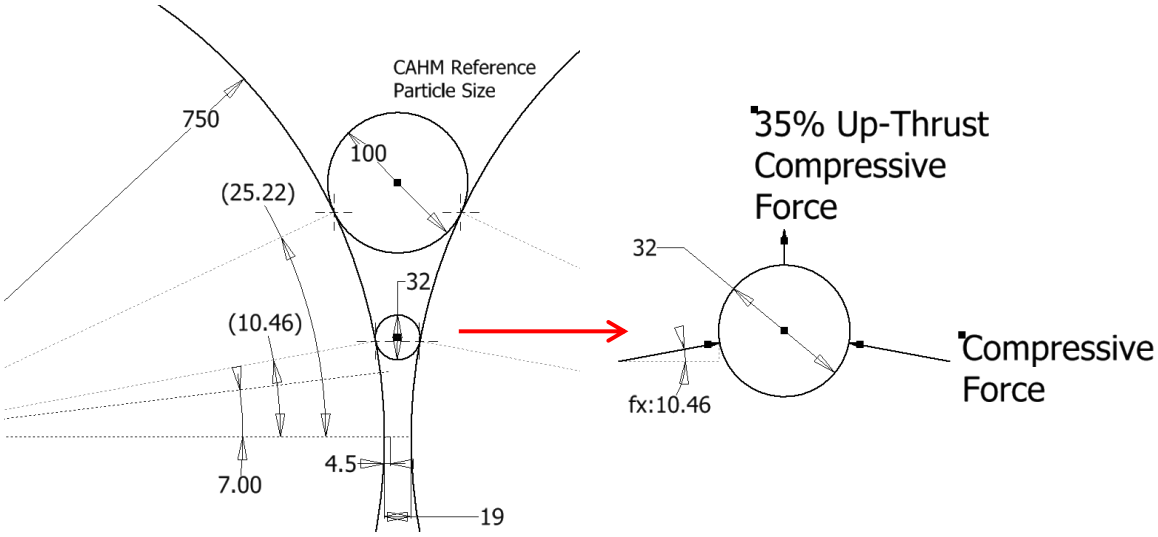

Figure 7: HPGR Nip Angle Configuration @ 19 mm operating gap illustrates 750 mm roller to 32 mm rock size, at 10.5 degrees above the horizon = 21 degree nip angle vs. CAHM with 100 mm rock reference comparison

We observe the HPGR ability to grasp and hold rock for breakage is limited to a ~24 degree included angle above horizontal, as indicated by our simulation of the UBC HPGR, Figure 7. This departs from published values of 14 degrees shown later in the presentation. Most designers of the HPGR assume all comminution occurs within a 7-degree arc above the horizon. DEM shows this to be an inaccurate assumption. Accepting DEM as an accurate portrayal of rock behavior, we found many other surprising points. We illustrate many facts to substantiate the claim.

There is an upward thrust force with large rock, nearing the machine size limit, as it approaches the critical nip angle. Figure 7 right-hand image illustrates the vector diagram of this condition. The upward force is equal to 35% of the compressive force. The surface texture and ore heap above the noted rock overcomes this thrust. There is a turbulent zone above this large rock size when the feed hopper geometry is not sufficiently narrow at the hopper discharge point.

HPGR has a 24 degree included nip angle at the noted rock-to-roller size ratio (32/750) = 0.043:1. Shear work wear does not become significant until the included angle reaches 14 degrees. This is also when the compression force magnitude is able to induce rock fracture and thus is the rock size limiting condition.

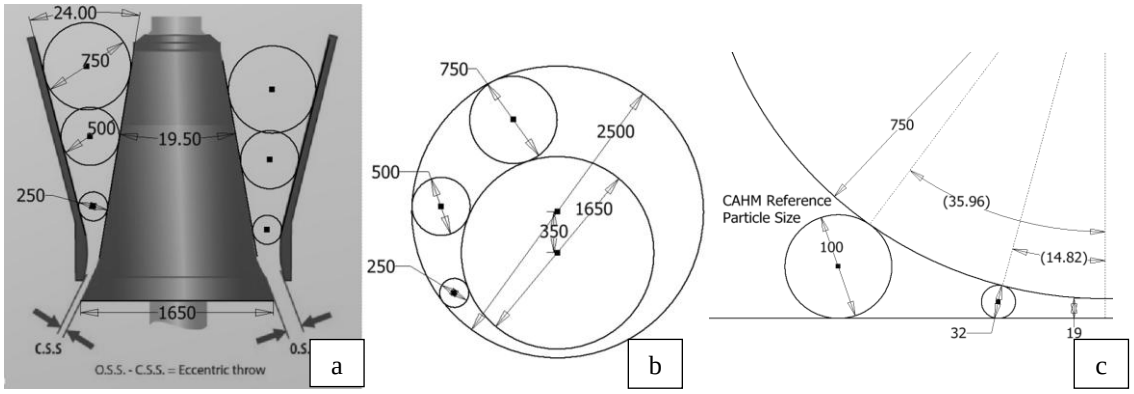

Figure 8a-b: Typical gyratory crusher illustrating the large 24-degree nip angle until the last ~500 mm vertical distance to its right is plan view; Figure 7c: VRM Configuration illustrated with vertical roller moving on a static horizontal plane, which cannot grab rock larger than a 12 degree nip angle, half the HPGR nip angle.

Figure 8 illustrates how the gyratory crusher works, with its large nip angle in elevation and plan view. It must establish a locking nip angle by heaving larger rocks until the rocks chip to geometry with a self-locking nip angles, which leads to added wear. Most crushers would benefit from creating a surface that does not induce excessive motion seen in most if not all crushers. Some have fluted mantles that help. I recall a Japanese gyratory supplier tested studs in their concave, but do not know how successful they were.

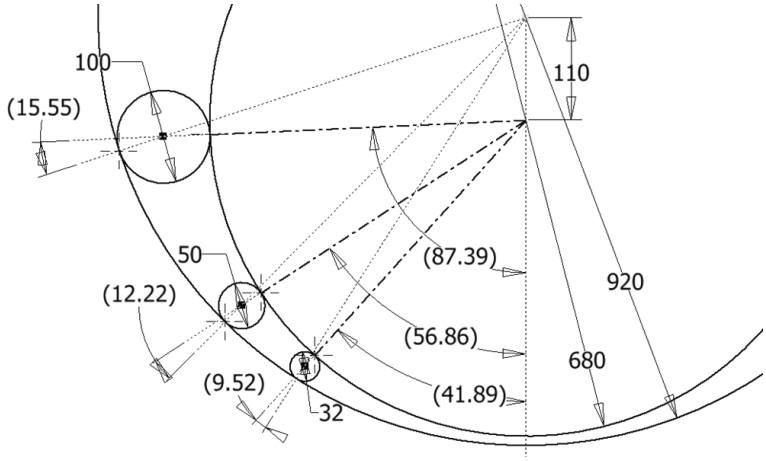

Figure 9: CAHM illustrating Positive Control of Rock Exclusive of Nip Angle

Figure 9 illustrates the CAHM Anvil and Hammer ring relationship with respect to rock nip angle. It can easily grab rock with a rock-to-roller size ratio > 0.18:1 or > 5:1 over the HPGR. In practice, this may be closer to 4:1 when considering stability and transient force magnitudes.

CAHM can apply many surface textures. We selected one arbitrarily, in Figure 1a, to demonstrate a piston-die rock containment crushing concept, and a way to maintain a high voidage between rocks to assure the highest comminution efficiency. Note, the approach path is long with a slow compression cycle compared to other comminution machines. Prof. Schönert says this produces optimal efficiency.

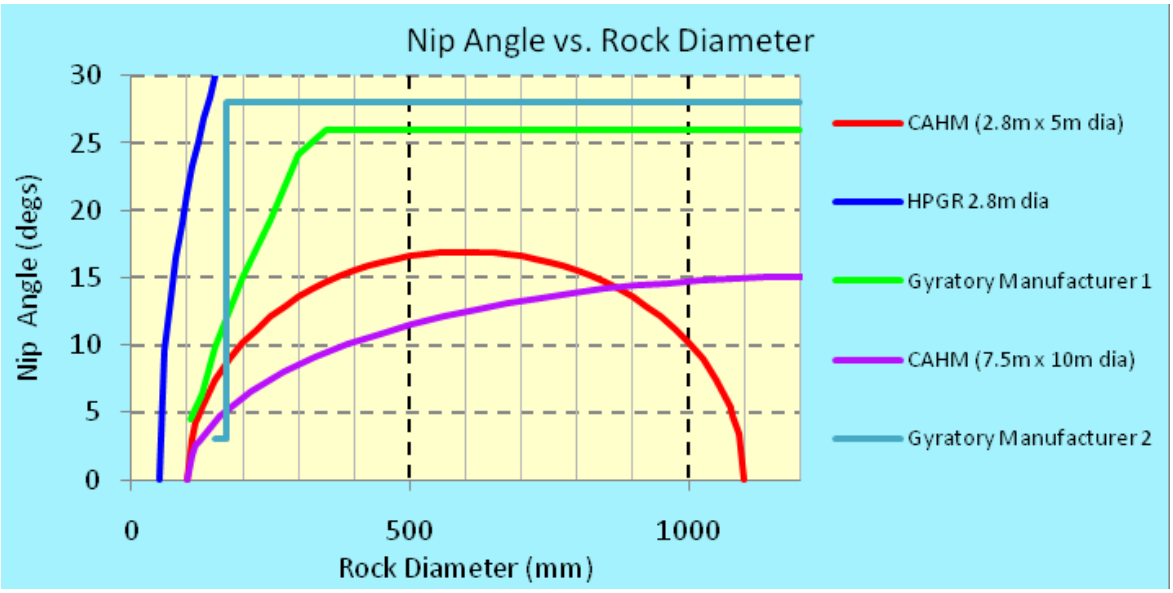

Figure 10: Nip Angle vs. Rock Diameter for Two Gyratory Crushers, HPGR, and Two CAHM Configurations

In Figure 10, we illustrate in one graph, nip angle comparisons vs. digestible rock size between HPGR, Gyratory Crushers, and CAHM machines of selected sizes.

The dark blue graph is a 2.8 m diameter HPGR. Aqua graph depicts one gyratory crusher supplier with an invariant nip angle with respect to rock size, while the green line shows another crusher supplier.

CAHM are the red and purple graphs with different hammer ring to anvil diameter ratios. Red hammer ring is 56% of anvil ring diameter. Purple hammer ring is 75% of anvil ring. If the red hammer had been 75% of anvil ring, its nip angle would not exceed 15 degrees.

Above shows, HPGR rock size limit is about 112 mm with a 2.8 m diameter and 24-degree nip angle. This follows the rock-to-roll diameter ratio = 0.04:1.

Key points of interest are:

a) Two known gyratory crusher suppliers with very different nip angles may also have very different performance,
b) HPGR with 2.8 m diameter rolls could have difficulty digesting rock bigger than 112 mm, due to the 24 degree nip angle limit that will not efficiently grab this size rock, or it must have a special large pin geometry,
c) CAHM, with same diameter of hammer ring as HPGR shown in red curve, can digest 370 mm rock with 15 degree nip angle (3.4:1 rock size benefit), and CAHM with 7.5 m diameter hammer ring can digest 1200 mm rock at 15 degree nip angle and reduce it to < 100 mm in one pass.

The red graph illustrates the nip angle potential of the CAHM machine where a rock starts into the machine at zero with 12 o'clock position and tends to a maximum nip angle when the rock is about midway, and then back to zero when the rock reaches 6 o'clock.

We believe the rock size limit will be about 17% of the difference in anvil to hammer ring diameters. The red graph, at 2.8 m roll size, could digest a rock size of about 370 mm. This will most likely depend on the machine stiffness and bearing supports.

ROCKY HPGR & CAHM MODEL SETUP PER TABLE 1 – HIGHLIGHTED IN YELLOW

We model HPGR and CAHM using a commercial DEM program to compare performance properties. The commercial code is called ROCKY. ROCKY can demonstrate performance differences including rock fragmentation, machine power, throughput, wear, forces, and acceleration dynamics.

ROCKY can simulate particles down to a very fine degree at the cost of simulation time and GPU memory. A reasonable particle size range of 32mm to 8mm is chosen for the feed material matching the PSD shown in Zorig Table 2 and plotted in Figure 12. The minimum breakage size down to 3mm also reduces the overall length of the simulation and does not drastically affect the overall simulation results. Zorig did not go into detail on the various particle shapes (number of facets, length to width ratios, etc.), so we assumed that a 10 faceted polyhedron with a 1:1:1, 3-D aspect ratio for all particles per Figure 11. As a result, the PSD will only match to a certain degree of resolution. Also omitted were tuning the particle-on-particle and particle-on-surface frictions, angle of repose, and angle of withdrawal, so assumptions were made using extensive experience with rock calibration.

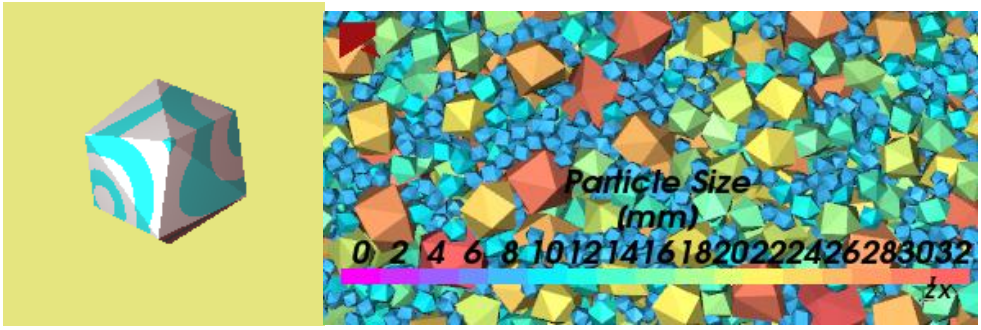

Figure 11: Particle Shape and Size with 10 facets left; at right is Table 2 PSD used for HPGR and CAHM simulations – yields a highly competent ore vs. a more slabby ore

Press constants	Roller diameter (D)	[m]	0.750						
	Roller width (W)	[m]	0.220						
Data	Description	Test number:		Au (C) 1	Au (C) 2	Au (C) 3	Au (C) 4	Au (C) 5	Au (C) 6
		Symbol	Unit						
Process set points	Speed	v	[m/s]	0.750	0.750	0.750	0.750	0.750	0.750
		n	[rpm]	19.10	19.10	19.10	19.10	19.10	19.10
	Static gap	X_0	[mm]	9.0	9.0	9.0	9.0	9.0	9.0
	Hydraulic pressure	P	[bar]	82	62	41	82	62	41
	Pressing force	F	[kN]	660.0	495.0	330.0	660.0	495.0	330.0
	Specific pressing force	F_{SP}	[N/mm^2]	**4.00**	**3.00**	**2.00**	**4.00**	**3.00**	**2.00**
Process data	**Test time**	t	[s]	15.28	12.83	16.37	15.93	17.10	16.73
	Average actual speed	ω_{AV}	[m/s]	0.83	0.77	0.80	0.80	0.80	0.81
	Standard deviation	σ_ω		0.40	0.20	0.28	0.33	0.32	0.32
	Actual roller gap (average)	X_{gAV}	[mm]	**18.24**	**18.72**	**20.53**	**20.20**	**20.65**	**22.25**
	Standard deviation	σ_X		0.48	0.52	0.73	0.31	0.36	0.26
	Actual hydraulic pressure (average)	P_{AV}	[bar]	**81.9**	**61.3**	**40.1**	**82.1**	**62.0**	**37.4**
	Standard deviation			0.47	1.95	0.73	0.38	0.40	0.84
	Actual pressing force (average)	F_{AV}	[kN]	659	493	323	660	499	301
	Actual specific pressure (average)	F_{SPAV}	[N/mm^2]	**4.00**	**2.99**	**1.96**	**4.01**	**3.03**	**1.83**
	Idle power draw	Pi	[kW]	10.96	10.62	10.39	9.87	9.66	9.74
	Power draw	P	[kW]	75.72	64.12	48.95	67.32	55.53	43.16
	Total specific energy consumption	E_{SP}	[kWh/t]	3.04	2.59	1.86	2.36	1.93	1.43
	Net Specific energy consumption	$E_{SP\,net}$	[kWh/t]	**2.60**	**2.16**	**1.47**	**2.01**	**1.59**	**1.11**
	Press throughput	W	[t/h]	**24.88**	**24.79**	**26.31**	**28.52**	**28.79**	**30.09**
	Specific throughput constant	m dot	[ts/hm^3]	**182**	**196**	**201**	**216**	**218**	**226**

Table 1: Gold (C) Ore from Zorig. pg. 224, Fig. A.2 [2]

		Centre		Edge		Full PSD	Feed		Scaled 90/10
Sieve range (mm)	Nominal size, (mm)	Retained (g)	Cum. Passing %	Retained (g)	Cum. Passing %	Cum. Passing %	Retained (g)	Cum. Passing %	Cum. Passing %
-35.5 +32	32	0	100.0	0.0	100.0	100.0	0	100.0	100.0
-32 +25	25	0	100.0	0.0	100.0	100.0	2462.9	69.3	100.0
-25 +19	19	131	99.0	214.3	97.6	98.5	1942.8	45.1	98.8
-19 16	16	364.1	96.1	678.9	90.0	94.2	889.4	34.0	95.5
-16 +12.5	12.5	778.4	90.0	1180.3	76.8	85.8	750.7	24.7	88.6
-12.5 +8	8	2407.9	71.0	2076.1	53.6	65.4	913.2	13.3	69.2
-8 +5.6	5.6	1372.2	60.2	1072.2	41.6	54.3	362.2	8.8	58.3
-5.6 +4	4	1301.4	49.9	799.5	32.7	44.4	191.8	6.4	48.2
-4 +2.8	2.8	1107.4	41.2	606.3	25.9	36.3	127.2	4.8	39.6
-2.8 +2	2	934.3	33.8	442.0	21.0	29.7	72.9	3.9	32.5
-2 +1.4	1.4	756.0	27.8	368.0	16.9	24.3	49.8	3.3	26.8
-1.4 +1	1	557.9	23.5	206.2	14.6	20.6	34.9	2.9	22.6
-1 +0.71	0.71	445.6	19.9	155.9	12.8	17.7	23.1	2.6	19.2
-0.71 +0.5	0.5	384.5	16.9	189.3	10.7	14.9	26.8	2.2	16.3
-0.5 +0.355	0.355	247.1	15.0	114.7	9.4	13.2	18.0	2.0	14.4
-0.355 +0.25	0.25	235.7	13.1	106.0	8.2	11.6	16.4	1.8	12.6
-0.25 +0.18	0.18	181.9	11.7	97.2	7.2	10.2	13.5	1.6	11.2
-0.18 +0.125	0.125	188.7	10.2	82.4	6.2	8.9	15.2	1.5	9.8
-0.125 +0.09	0.09	145.6	9.0	103.8	5.1	7.8	11.3	1.3	8.6
-0.09 +0.063	0.063	150.9	7.8	73.7	4.3	6.7	15.9	1.1	7.5
-0.063 +0.045	0.045	132.8	6.8	42.4	3.8	5.8	11.9	1.0	6.5
-0.045	-0.045	862.2		338.2			78.0		
Total mass		12685.6		8947.4			8027.9		
	P 80		10.14		13.34	11.22		27.44	10.49
	P 50		4.01		7.27	4.91		20.21	4.29

Table 2: Feed and Product data for Au (C) 3 from Zorig. pg. 227, Fig. A.7 [2]

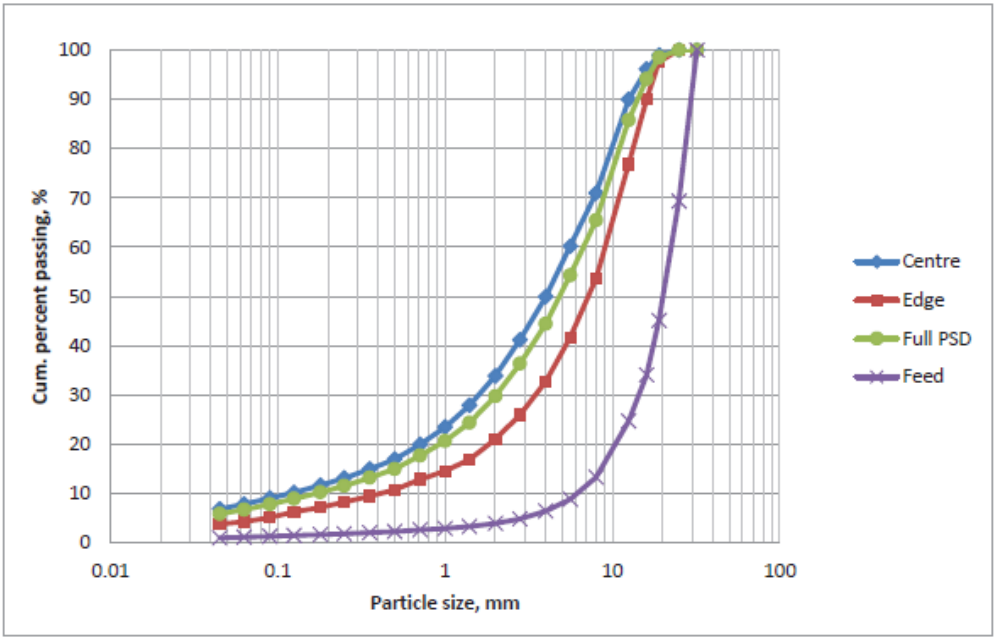

Figure 12: Plotted PSD for Au (C) 3 from Zorig. pg. 227, Fig. A.7 [2]

The remaining simulation parameters were taken directly from Table 1 using the following actual recorded data during the pilot testing.

	HPGR	CAHM (Inner Ring)
Initial Static Gap [mm]	9	6-10
Surface Speed [m/s]	0.8	1.89
Rotational Velocity [rpm]	20.4	60
Initial Pressing Force [kN]	323	300-800

Table 3: ROCKY Simulation input parameters for HPGR and CAHM

To simulate the HPGR gap variation in ROCKY, the pressing force is applied to the right-hand roller and given the degree of freedom to slide in the X-direction per gap reaction. The rotational velocity applied is constant for both rollers. ROCKY does not have a defined motor slip curve. This is an IP product of HPGR suppliers. This results in slightly noisy power readings, but the average power is still accurate. The same goes for the CAHM rotational speeds. The 1:1:1 aspect ratio will tend to exhibit a harder rock.

Results

The results of the pilot scale model simulated in ROCKY, plotted in Figure 14 through Figure 21, indicate that the lack of fine particles and inaccurate assumptions for rock strength and shape lead to inexact results to some degree. The resulting gap simulated is low, throughput is low, and the power low by less than 5%. The PSD shows that the rock used gives sufficient results to compare HPGR vs. CAHM. The gap, throughput, and power appear stable after 2 seconds of simulation. The crushed product shown in Figure 13 is tracked for tonnage and PSD after passing through the 9 mm simulation gap at piston force = 1.96 N/mm2. Figure 17 illustrates the HPGR and CAHM PSD fit vs. laboratory results.

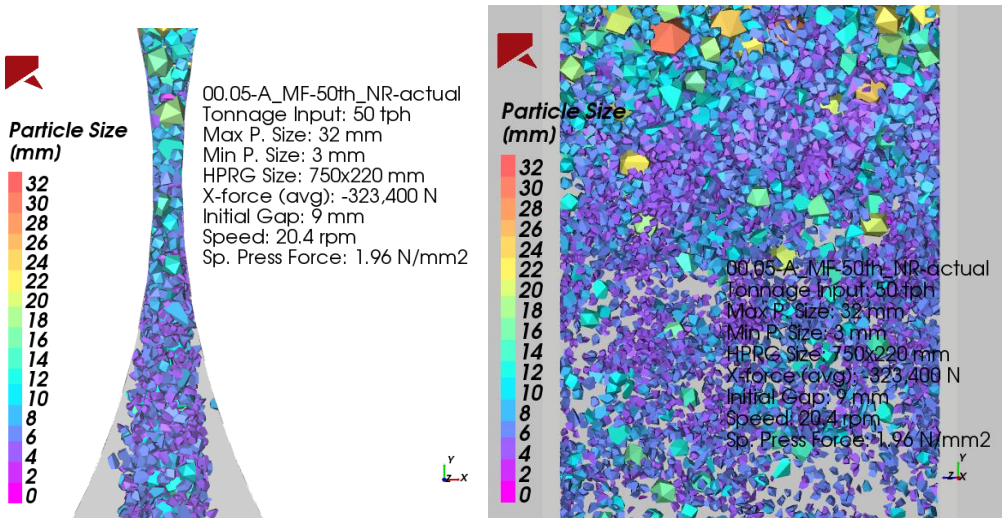

Figure 13: Product Front and Side Views

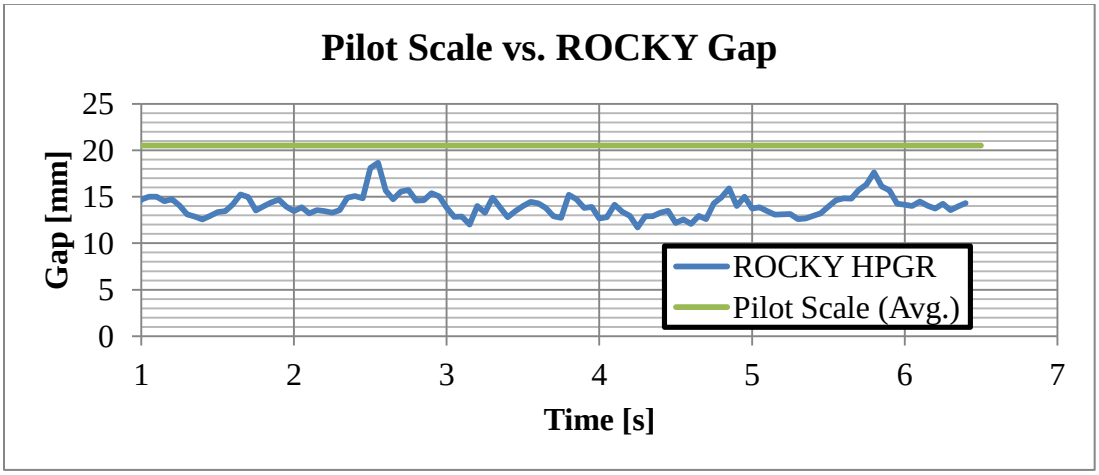

Figure 14: Gap Plot for HPGR

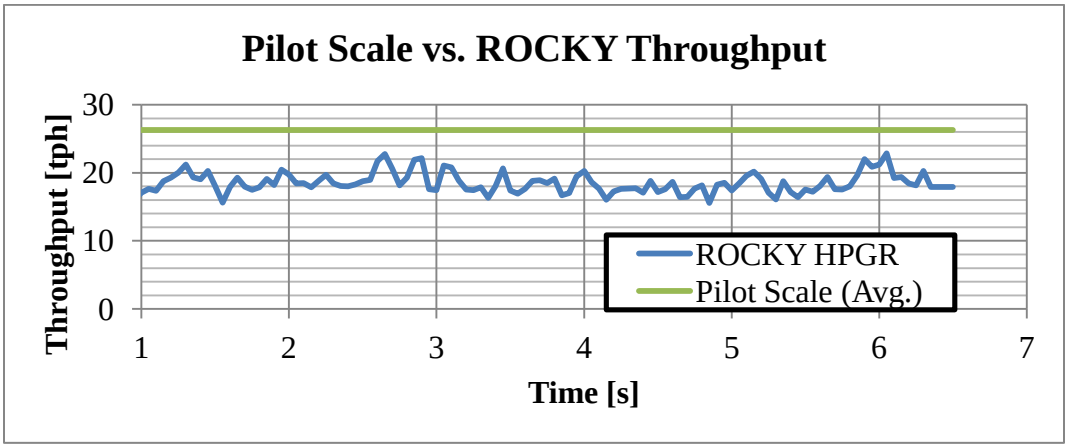

Figure 15: Throughput Plot

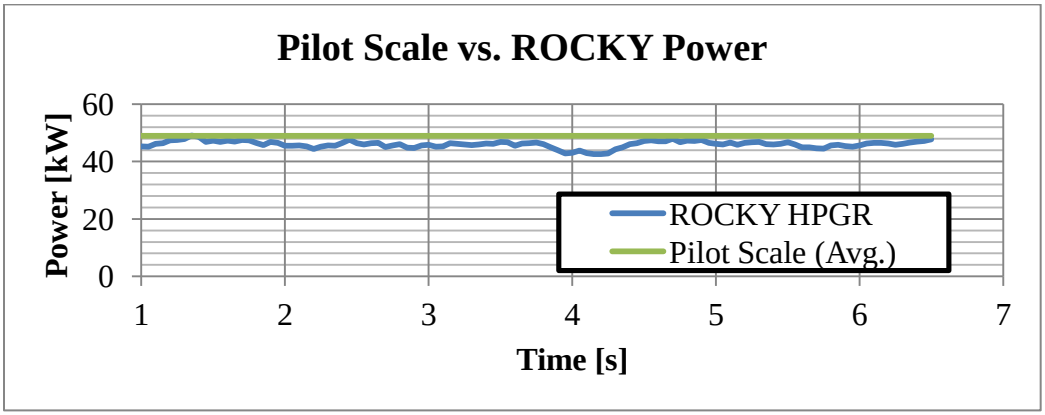

Figure 16: Power Plot

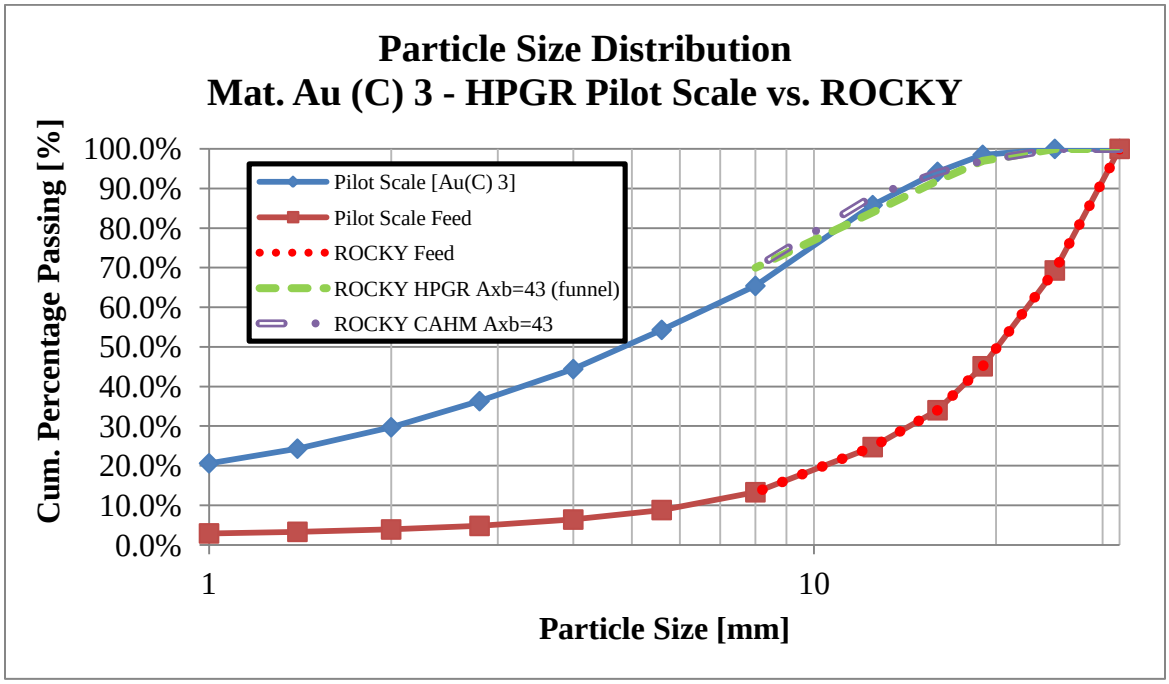

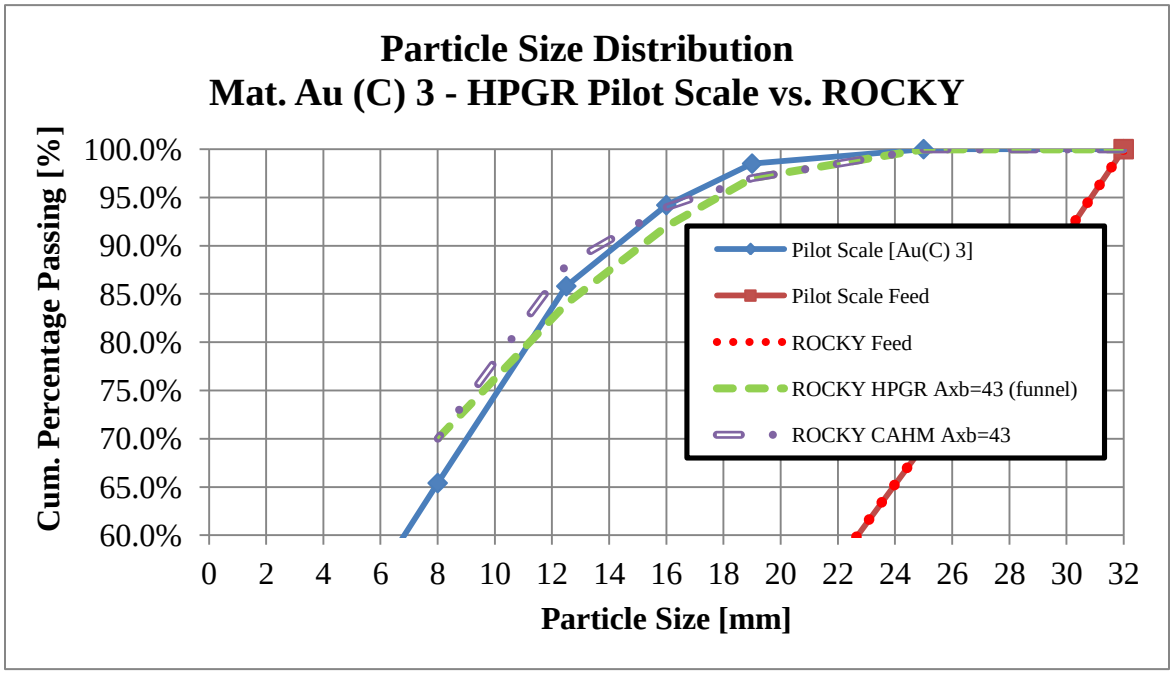

Figure 17: Particle Size Distribution Plot for UBC 750 mm dia. HPGR and 650 mm dia. CAHM fed with same ore and simulated by ROCKY code vs. Laboratory Measurements with feed and discharge results

ROCKY simulated feed and discharge was truncated, eliminating feed size below 8 mm. DEM breakage simulation was carried out to 3 mm, but the feed size became too large a particle set by the DEM simulation in the available time for the paper. However, we show the model can track breakage for HPGR and CAHM to a reasonable degree. We compare different machines with actual test results and against each other to validate claims of possible comminution efficiency and other improvements.

Observations

The material chosen is harder than the recorded values for this particular study by about 5%. This is, in part, due to the usage of average parameters for speed and applied force, and the use of a constant velocity for the rolls vs. motor slip response. Also affecting the overall outcome is the chosen A x b values as shown in the PSD plot in Figure 17. The values are somewhat suspect.

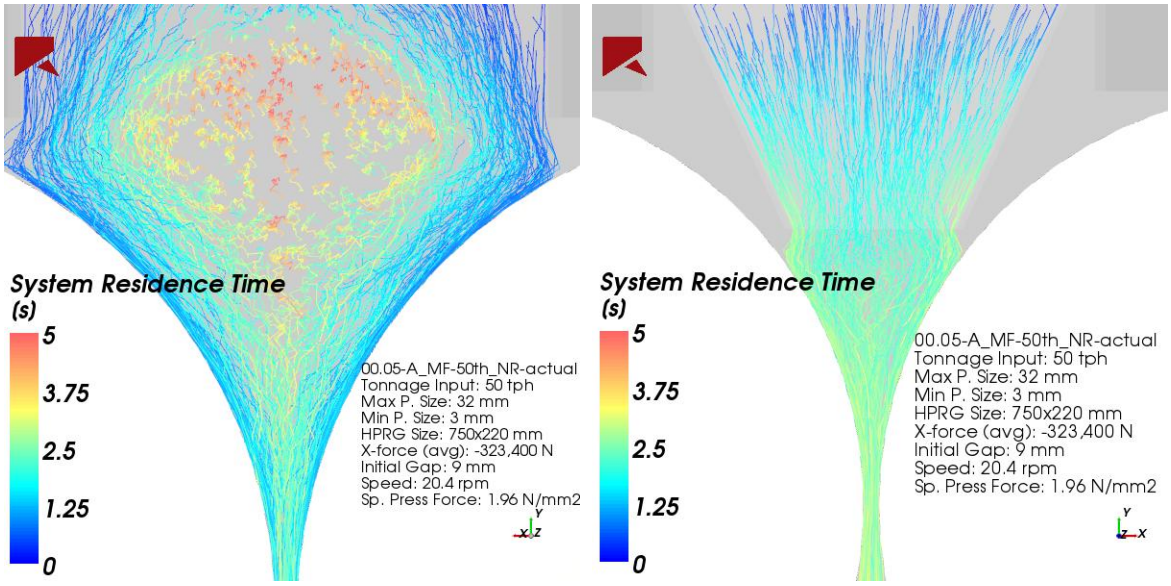

Figure 18: Particle Trajectories Visualized by Particle Residence time for HPGR: Wide Feed and Funnel Feed

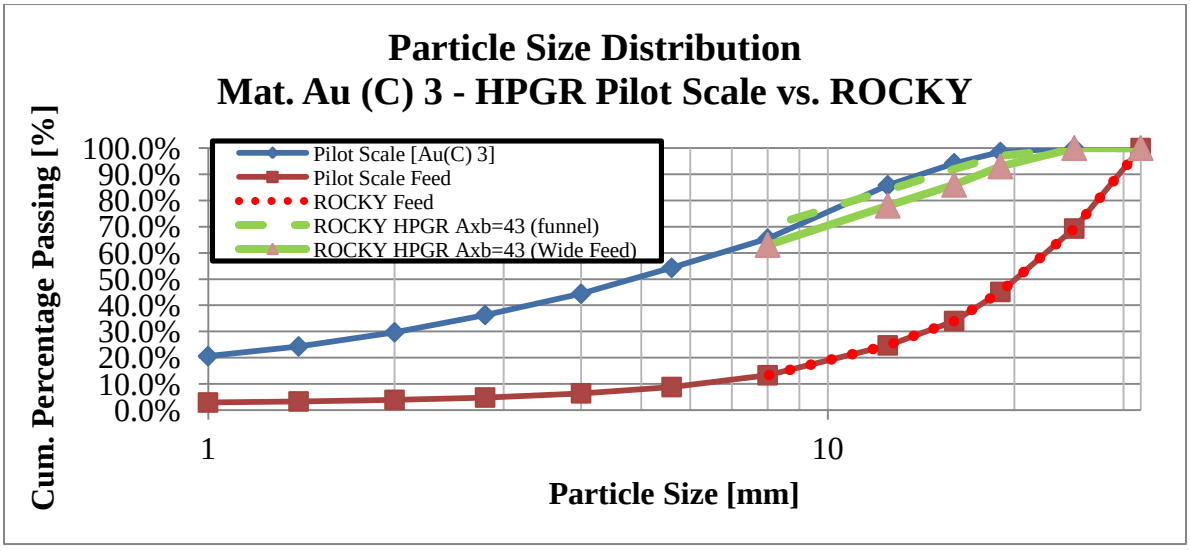

Figure 19: Particle Size Distribution for HPGR: Wide Feed and Funnel Feed

Figure 18 and Figure 19 illustrate results of two different feeder arrangements for the HPGR. The Wide Feed has a recirculation zone that prevents larger particles from entering the breakage area. Funnel Feed allows all particles to reach the breakage zone producing the expected PSD. In Figure 19, HPGR wide feed reduces the PSD curve by about 8% (62% passing wide; 70% passing funnel).

The funnel flow more closely mimics the laboratory results.

HPGR COMMINUTION PERFORMANCE – DEM vs. EXPERIMENTS

DEM simulation is validated and calibrated with UBC Piston-Die and Köppern HPGR test results.

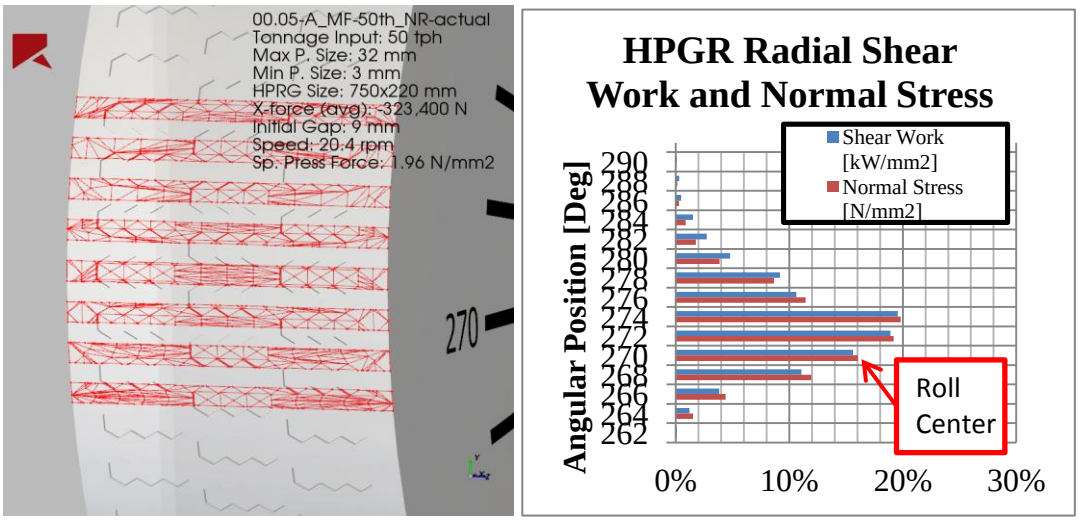

Figure 20: HPGR Radial Shear Work and Normal Face Pressure for test at UBC as defined by DEM

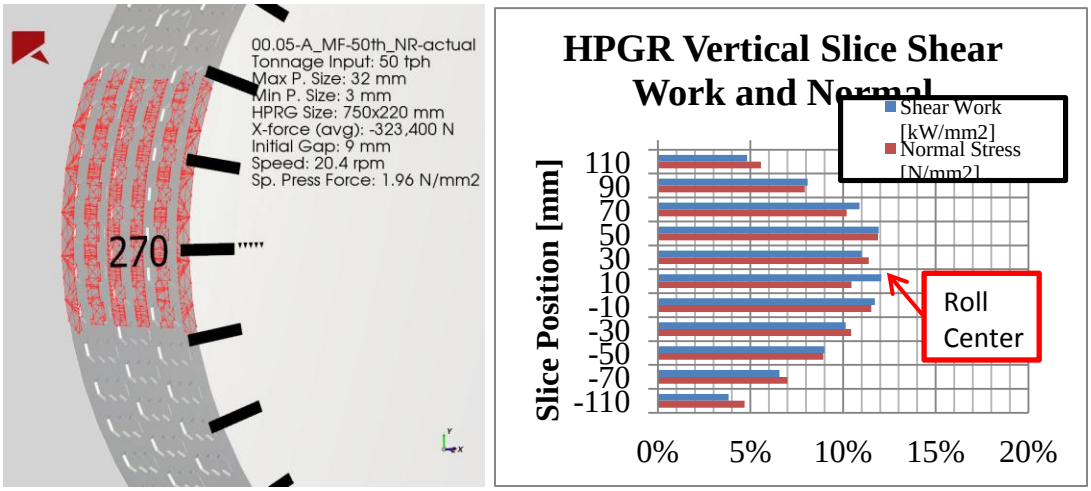

Figure 21: HPGR Vertical Shear Work and Normal Face Pressure for test at UBC as defined by DEM

Normal stress breaks the rock and shear stress wears the machine surface with unknown breakage effects. ure 20 and Figure 21 illustrate the DEM Normal Force (N/mm^2) and Shear Work (kW/mm^2) over the HPGR roll contact area. Note, maximum shear is 4 degrees above the horizon at the center of the roll face and the sliding roll shows slightly higher shear work than the fixed roll. About 16% of the total shear work occurs below the horizon by 4 degrees. The working arc of contact for the ore is about 18 degrees consisting of 12 degrees above the horizon and 6 degrees below the horizon.

CAHM DEM SIMULATION & COMPARISON TO HPGR

We simulate the CAHM machine with the identical feed as the HPGR from the UBC study.

The hammer ring diameter is configured similar to the HPGR roller, except the hydraulic pistons are pushing downward not horizontally. Therefore, CAHM gains force from the mass of the roll that augments the piston force. For this study, we applied a piston force of 6 kN over the roll width of 300 mm.

There are three identical internal Hammer Rings each 100 mm wide. Each hammer ring has sixteen identical piston geometries. Each piston has a 60 mm deep protrusion that mates with the Anvil Ring die pocket. At the bottom of each die, a slotted port is configured to release rocks that are broken below the critical slot opening. The Anvil Ring has sixty pockets or dies (twenty around, three wide) which mate with a hammer ring protrusion for each rotation. Anvil Ring captures all rock that falls into its pocket. The mating hammer ring piston then crushes rock. Each ring rotates on its own axis. The outer Anvil ring outer shell is supported by hydrostatic bearings.

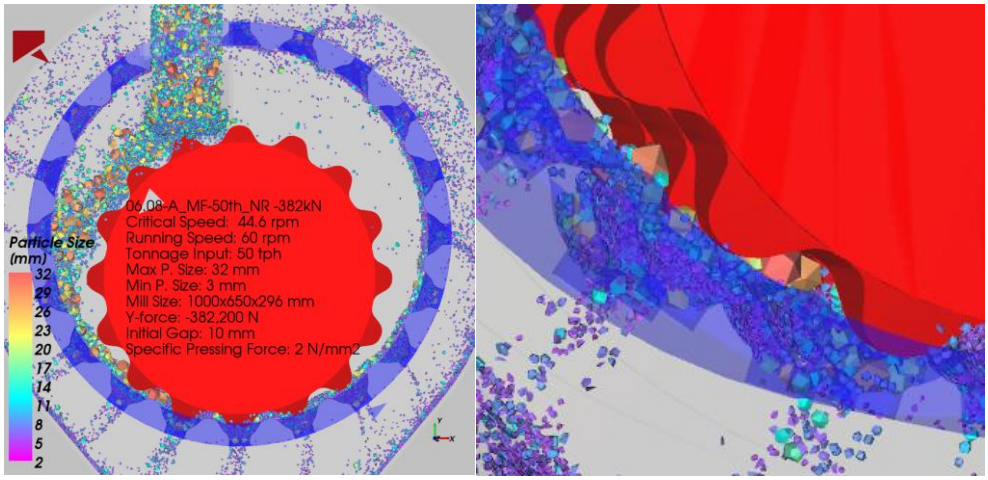

Figure 22: CAHM Feed and Product using Slotted Ports

Figure 22 shows the working CAHM machine continuously discharging material due to the super critical speed and the design of the ports. We did not optimize the hammer and anvil configuration. It produces better results than the HPGR design in terms of Specific Energy, PSD, and wear mechanics. The ratio of the hammers to anvils as well as the number of ports across the width can vary altering the throughput and life of the machine as well as the energy required. The size of the machine chosen for this study equates to the Pilot Scale HPGR used by UBC in terms of scale and used the same feed material.

Note, that the ports must first be primed with material on the first pass in order to reach a steady state. We consider this while analyzing the PSD and wear profiles.

We illustrate in Figures 23-25 the relative gains CAHM produces over the HPGR.

Figure 23 CAHM gap is constant 10 mm held by the piston restraint. Figure 24, CAHM shows a 54 t/h throughput vs. HPGR 19.5 t/h. Figure 25, CAHM requires 68 kW while HPGR requires 48 kW. CAHM PSD shows a 4% finer grind. CAHM Energy efficiency is 1.26 kW-hr/ton while the HPGR is 2.46 kW-hr/ton.

SUMMARIZING:

CAHM requires 50% of HPGR power to produce the same throughput.

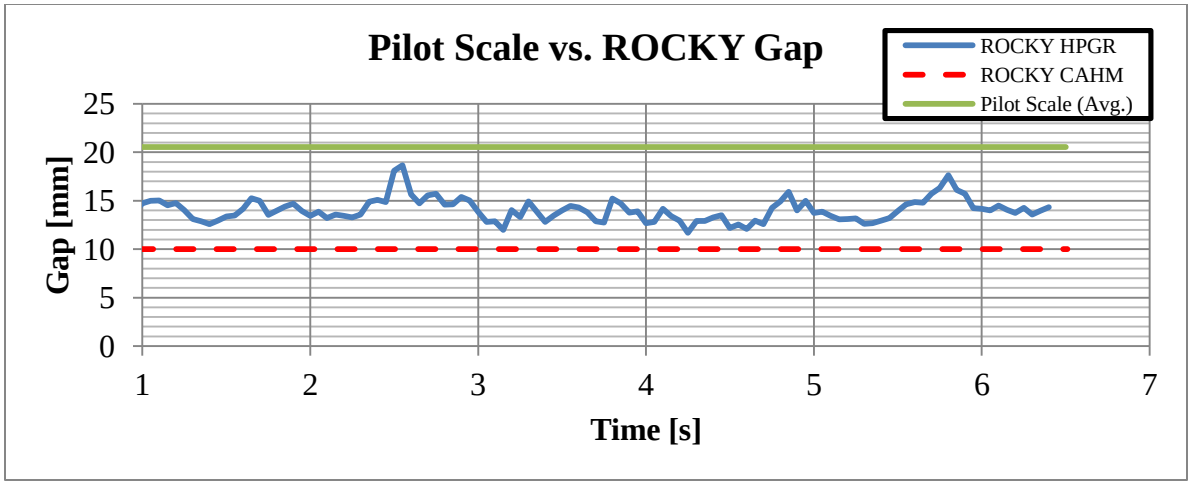

Figure 23: Gap Plot for HPGR vs. CAHM

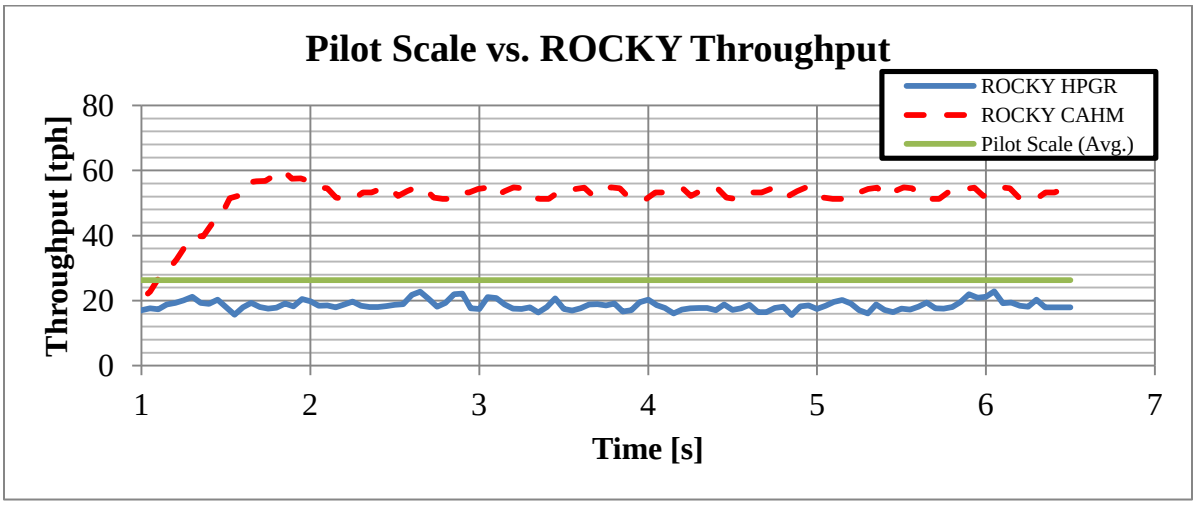

Figure 24: Throughput Plot for HPGR vs. CAHM

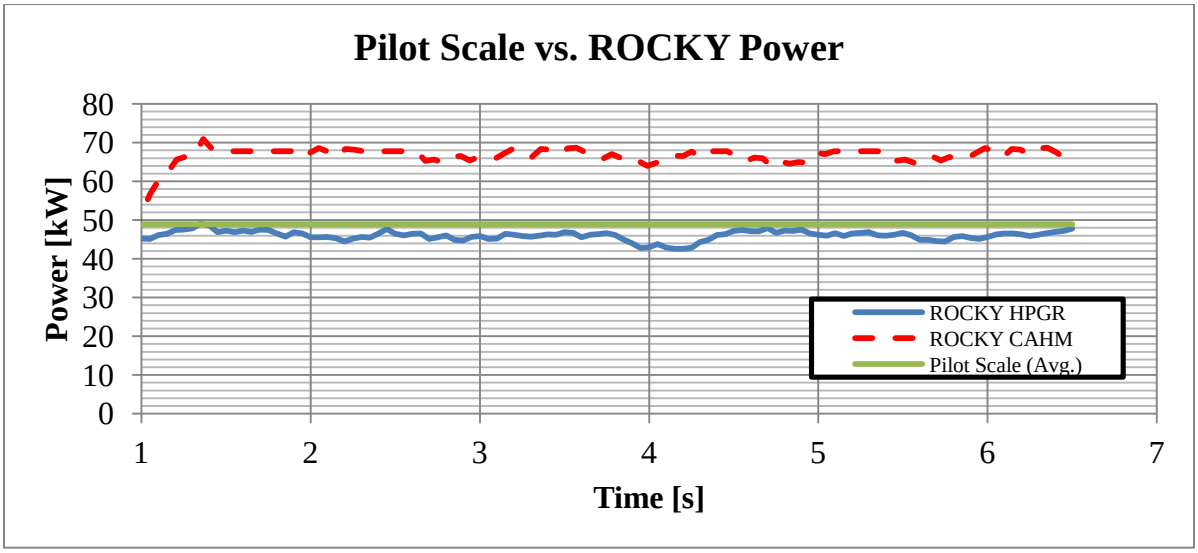

Figure 25: Power Plot for HPGR vs. CAHM

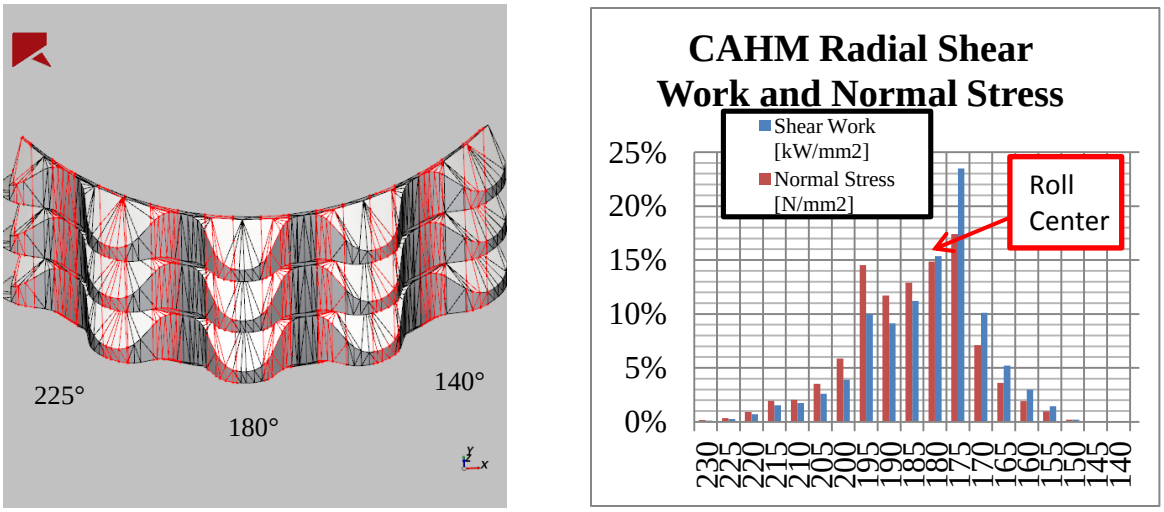

Figure 26: Plot of CAHM Radial Shear Work and Normal Face Pressure across face defined by DEM

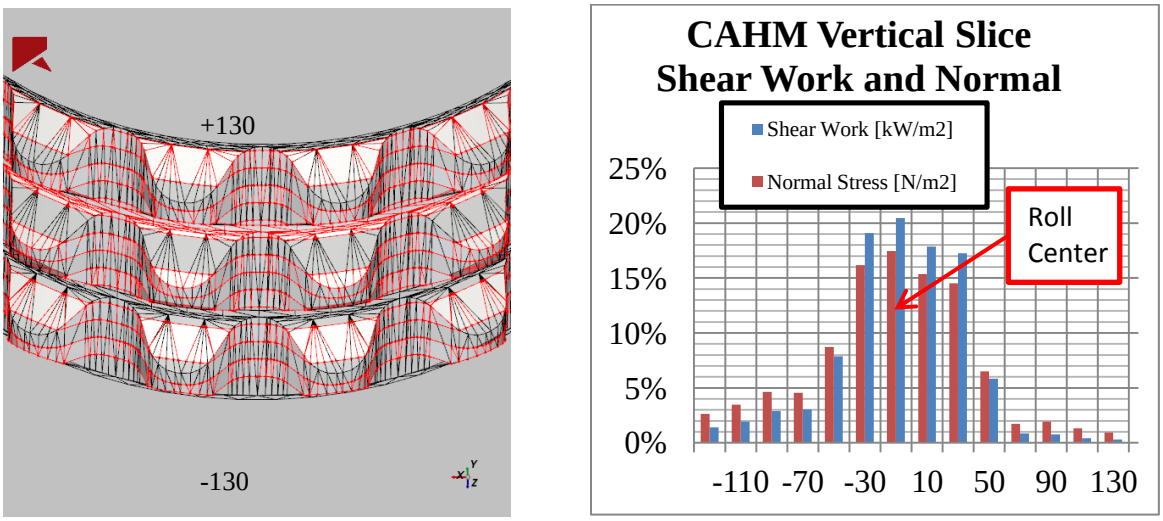

Figure 27: Plot of CAHM Vertical Shear Work and Normal Face Pressure contact arc defined by DEM

Figure 26 and Figure 27 illustrate the DEM Normal Force (N/mm^2) and Shear Work (kW/mm^2) over the CAHM inner ring contact area similar to the HPGR. CAHM work zone is approximately 40 degrees vs. HPGR 18 degrees. Note, the vertical slice arrangement recorded much higher shear and normal stress for the center of the machine due to poor chute loading of the initial feed material. This error can be corrected using angled feeder chutes and internal deflectors that evenly distribute the material..

Furthermore, the shear work over the respective surface areas shown in Figure 20 and Figure 21 for the HPGR is 0.027 kW/mm^2 vs. 0.0045 kW/mm^2 for the CAHM shown in Figure 26 and Figure 27, a reduction of wear by a factor of 6:1in favor of the CAHM. Correction to rock feed distribution will further enhance CAHM wear performance.

CONCLUSION

We quantify, using DEM analysis techniques, HPGR Specific Energy, Throughput, Wear Magnitudes, Wear Patterns, and Particle Size Distribution. We identify rock flow over the wear surfaces that can calibrate metal attrition. A high degree of accuracy is achieved by calibrating DEM with laboratory measurements.

This translates to all types of comminution machines. Processes can quickly and inexpensively be analyzed using Pilot Scale testing to then build full scale models within DEM.

Although the throughput and gap comparison between the simulation for the HPGR and the Pilot Scale test were less accurate than power and PSD results, there is some suspicion the A x b values contribute to the error. Considering the degree of accuracy, ROCKY can be used as a proof of concept to further develop an understanding of currently used crushing devices and revisit new machines such as the CAHM or Piston-Die arrangements as shown in this report.

CAHM proved to be ~50% more efficient than the HPGR for throughput over power consumption at 1.23 kW-hr/ton.

CAHM reduces metal surface wear to 20% of the HPGR. CAHM approaches the more desirable piston-die action than the HPGR. Pressure relieving discharge ports yield further improvements.

CAHM's can apply much higher rock pressure without reducing throughput or significantly increasing power draw. CAHM has other optional designs of the hammer/anvil shape that produce other benefits. A change in port geometry leads to a change in PSD. Further investigation using a finer feed and a smaller minimum grind size would reveal more detail on the PSD at the cost of simulation time.

CAHM results prove the importance of maintaining high voids between particles and the effects of utilizing longer approach angles.

CAHM selected for this study is of a similar size to the HPGR Pilot Scale in order to deliver a proof of concept. CAHM Size and shape variable, number of ports, ratio of anvil pockets (dies) to hammers (pistons), operating speed, Specific Force applied, etc., are virtually limitless. Variable geometry selections depend on the desired product, operating cost, and comminution efficiency.

Further research into a physical wear model simulation using ROCKY can help determine the weak points in the design and can identify how the PSD changes over time. As shown above, using simple piston-die arrangements can optimize the size and shape of the anvil, hammer, and slot shapes. Laboratory tests will guide design of most appropriate material selections.

BIBLIOGRAPHY

[1] K. Schonert, "A first survey of grinding with high-compression roller mills," Vols. 22. 401-412, 1988.

[2] Z. Davaanyam, "Piston Press Test Procedures for Predicting Energy-Size Reduction of High Pressure Grinding Rolls," UBC, Vancouver, 2015.

[3] L. Nordell, "Conjugate Anvil-Hammer Mill". US Patent US201234952 A1, 20 Sep 2012.

[4] T. J. Napier-Munn and et. al., Mineral Comminution Circuits, Indooroopilly: JKMRC, 2005.

[5] D. A. Potapov, *Rocky,* [Computer Software] Ver. 3.9.1: ESSS <http://rocky-dem.com/>, 2016.

[6] W. Contributors, "Voronoi Diagrams," Wikipedia, The Free Encyclopedia, [Online]. Available: https://en.wikipedia.org/w/index.php?title=Voronoi_diagram&oldid=712984705. [Accessed 6 April 2016].

[7] S. Nadolski, B. Klein and et. al., "Development and application of an energy benchmarking model for mineral comminution," *SAG,* 2015.

[8] J. T. Kalala, H. Dong and A. L. Hinde, "Using Piston-Die Press to Predict the Breakage Behavior of HPGR," Comminution Group, Minerals Processing Division, MINTEK, Randburg, South Africa, 2015.

[9] M. S. Powell and L. X. Liu, "New approach on confined particle bed breakage as applied to multicomponent ore," *Minerals Engineering,* no. 85, pp. 80-91, 2016.

[10] M. S. Powell, L. M. Tavares and et. al., "The appropriate, and inappropriate, application of the JKMRC t10 relationship," *IMPC 2014,* p. 747.

[11] K. Schonert, "The influence of particle bed configurations and confinements on particle breakage," *Mineral Processing,* Vols. 44-45, pp. 1-16, 1996.

[12] K. Schonert and J. Liu, "Modelling of interparticle breakage," *Mineral Processing,* Vols. 44-45, pp. 101-115, 1996.

[13] R. Chandramohan, G. S. Lane and et. al., "Reliability of some ore characterization tests," Ausenco report, Brisbane, 2015.

[14] E. Oberg and F. D. Jones, Machinery's Handbook, New York: The Industrial Press, 1964.

[15] D. A. Mishra and et. al., "Rock failure modes under uniaxial compression, Brazilian, and point load tests," [Online]. Available: https://www.researchgate.net/publications/258845369. [Accessed 7 Feb. 2016].

[16] M. J. Daniel, "Particle bed compression comminution using a piston-die to predict the performance of HPGR," JKMRC.